Received April 15, 2020, accepted April 28, 2020, date of publication May 6, 2020, date of current version May 15, 2020.

Digital Object Identifier 10.1109/ACCESS.2020.2991689

A Novel Adaptive Control Method for Performance Enhancement of Grid-Connected Variable-Speed Wind Generators

MAHMOUD A. SOLIMAN[1], HANY M. HASANIEN[2], (Senior Member, IEEE), AHMED AL-DURRA[3], (Senior Member, IEEE), AND IBRAHIM ALSAIDAN[4]

[1]Electrical Engineering Department, Faculty of Engineering, Menoufiya University, Shebin El-Kom 32511, Egypt
[2]Electrical Power and Machines Department, Faculty of Engineering, Ain Shams University, Cairo 11517, Egypt
[3]Advanced Power and Energy Center, EECS Department, Khalifa University of Science and Technology, Abu Dhabi, United Arab Emirates
[4]Department of Electrical Engineering, College of Engineering, Qassim University, Buraydah 52571, Saudi Arabia

Corresponding author: Mahmoud A. Soliman (dr.msoliman08@gmail.com)

ABSTRACT Huge penetration of grid-tied wind generators into the existing electricity networks increased various challenges in modern power grids. Tremendous attempts are accomplished to properly enhance the behavior of the wind generation systems. This article exhibits a new self-tuned control approach for enhancing the performance of a permanent-magnet synchronous generator-based wind turbine, which is interlinked to the electricity network. The self-tuned technique relies on an improved multiband-structured subband adaptive filter (IMSAF) algorithm, which achieves less computational intricacy over the least-mean-square approach. The IMSAF algorithm-based self-tuned proportional-integral (PI) controller is employed to adjust the interface voltage source converters through a cascaded control structure. The IMSAF algorithm updates the multiple PI controllers' gains on-line without the necessity to optimize or fine-tune. To achieve realistic responses, practical wind speed data measured in Zaafarana wind farm, Egypt, are implemented in this study. The efficacy of self-tuned control approach is compared with that realized using an optimized PI control approach by the water cycle and the genetic algorithms, considering symmetrical and unsymmetrical faults, as the network disturbances. The validity of self-tuned control approach is widely confirmed by performing simulation analyses using MATLAB/Simulink software, and satisfactory responses are achieved. Notably, the IMSAF-based self-tuned control approach is realized to be an accurate means for improving the characteristic of grid-tied wind generators.

INDEX TERMS Adaptive control, adaptive filter algorithm, power converters, power system control, power system dynamics, wind energy.

NOMENCLATURE

ABBREVIATIONS

AF	Adaptive filter
CCS	Cascaded control strategy
CMPN	Continuous mixed *P*-norm
DFIG	Doubly-fed induction generator
FC	Frequency converter
GSI	Grid-side inverter
IMSAF	Improved multiband-structured subband adaptive filter
MSC	Machine-side converter
OVPS	Over-voltage protection scheme
PCC	Point of common coupling
PMSG	Permanent-magnet synchronous generator
PLL	Phase-locked-loop
PI	Proportional-integral
RECS	Renewable energy conversion system
SRG	Switched reluctance generator
SEIG	Self-excited induction generator
VSWT	Variable-speed wind turbine
VS-WTGS	Variable-speed WTGS
VSC	Voltage source converter
LMS	Least-mean-square

The associate editor coordinating the review of this manuscript and approving it for publication was Ruisheng Diao.

WCA	Water cycle algorithm
WT	Wind turbine
WTGS	Wind turbine generator system

SYMBOLS

ρ	Air density
V_{dc}, V_{dc}^{*}	DC-link voltage and its set-point value
ω_e	Electrical angular speed of PMSG
v_{ds}, $v_{qs}\lambda_{\text{opt}}$	d- and q-axis stator voltages of PMSG
i_{ds}, i_{qs}	d- and q-axis stator currents of PMSG
L_d, L_q	d- and q-axis self-inductances of PMSG
J	Moment of inertia of PMSG
λ_m	Magnetic flux of PMSG
P_ω	Mechanical power extracted from WT
M_{us}	Maximum undershoot
P_{opt}	Optimum power of the WT
M_{os}	Peak overshoot
P	Pole pair number of the PMSG
Q_{PCC}	Reactive power at the PCC
R	Radius of the WT's blade
P_{PMSG}, Q_{PMSG}	Real and reactive powers of PMSG
ω_r	Rotational rotor speed of the WT's shaft
R_s	Stator resistance of PMSG
L_s	Synchronous inductance of the PMSG
E_{ss}	Steady-state error
T_s	Settling time
λ, λ_{opt}	Tip speed ratio and its optimum value
β	Turbine blade Pitch angle
θ_r	Transformation angle of the PMSG
θ_t	Transformation angle of the grid
V_{PCC}	Terminal voltage at the PCC
C_P, C_{P-opt}	WT Power coefficient and its optimum value
V_w	Wind speed

I. INTRODUCTION

Over the last decades, various renewable energy technologies, including wind, solar, wave, tidal, and geothermal energy have generated significant attention worldwide due to several strategic factors, including the exhaustion of fossil fuel, global warming, political matters, and propensity to live in a healthy environment. Owing to its huge energy generation capability with minimal expenses and its minimum climate effect, wind energy has tremendous potential to act a vital role in the modern electric power systems. Globally, the installed wind power realized 591 GW in 2018, representing an increase of 9.6% compared to 2017's statistics [1]. According to the recent records, it is anticipated that the installed wind power will achieve 917 GW worldwide by 2030 [1]. With large-scale permeation of wind power plants into the exciting power system, different problems have been released, which must be addressed, inspected, and solved. Therefore, it is indispensable to explore the transient and dynamic behaviors of a grid-interlinked WTGS to enhance its performance.

At present, the VS-WTGS technologies have become more trustworthy for the wind generation sector. This significant attention is because of their distinguished features, such as higher power capture, lower quantities ripple, and a high degree of controllability over that of the fixed-speed [2], [3]. Various classes of electric generators-based VS-WTGSs are commercially obtainable in the wind power market [4]. SRG is made of magnetic core and windings, which has a simple and robust structure. However, it requires an excitation circuit and a position sensor, leading to a complicated circuitry [4], [5]. SEIG is distinguished by its brushless structure, simple operation, and good dynamic behavior. But, it suffers from the regular maintenance of the gearbox and the high cost of capacitor-bank required for the excitation. Besides, SEIG has poor voltage and frequency regulations, where it depends on excitation capacitance and prime mover speed [6], [7]. Moreover, DFIG is widely utilized in large-scale WTGS due to its lower converter costs and lower power losses. However, its demerits are the limited speed range and the regular maintenance for gearbox and slip-rings [8]–[10]. On the other hand, PMSG is the most efficacious and favorable technology applied in the VS-WTGS [11]–[14]. This technology becomes more expectant for modern wind generation system worldwide [12]. This solicitude is due to its salient features such as the self-excitation, which allows higher power factor operation and high efficiency. In addition, PMSG has a small size compared to its power rating and has a grid support capability [13]. Moreover, PMSG has multi magnetic poles and large air gaps, resulting in low rotational generator speed [2]. In a direct-drive PMSG configuration, the gearbox can be omitted, leading to lower losses/cost and higher reliability [13], [14]. Moreover, due to the absence of the magnetization current, PMSG is more appropriate than other electric machines.

The VSWT driving a PMSG, as a rule, is integrated into the electricity network using a full-rated FC that involves two VSCs linked by a DC-bus capacitor [2], [15]. This topology presents distinct merit, where the FC decouples the generator from the power grid. Hence, the network fluctuations/disturbances have no direct impact on the generator. As a result, WTGS performance can be further enhanced. In addition, the full-rated FC provides a better control capability over system variables.

The well-designed CCS is considered a good candidate here to control the VSCs of the grid-tied WTGS [16], [17]. This control structure relies, in general, on the PI controllers. These controllers are still widespread in various industrial systems because of their features, including the system robustness, the simple design, and the extensive stability margins. But, the PI controllers encounter some problems, such as the high instability to the nonlinear dynamic systems and variables' variation [2], [17], [18]. Various research studies have been employed with the proper designing of multiple PI controllers to improve the performance of grid-tied WTGSs. The PI controller was employed to adjust an energy storage

system to properly enhance the behavior of VS-WTGSs [19]. Moreover, several control approaches have been suggested to reinforce the WT stability [20], [21]. Notably, the PI controller has been widely utilized in different control approaches for various RECSs [22]–[24]. In these previous studies, the design of such controller relies on the trial and error criteria, which requires a long period, extremely huge efforts, and essentially depends on the designer expertise. Hence, the fine-tuning of these controllers reveals an extreme challenge to the control designers, particularly in large nonlinear systems.

Recently, various optimization techniques are presented to optimally design the multiple PI controllers' gains [25]–[27]. Shuffled frog leaping algorithm [16], harmony search algorithm [28], grey wolf optimization [2], whale optimization algorithm [29], gravitational search algorithm [30], WCA [17], [31], and mine blast algorithm [32], modified selfish herd optimization [33], and quasi-oppositional selfish-herd optimization algorithm [34] were proposed for properly designing the multiple PI controllers through the CCS for enhancing the performance of RECSs. Significant enhancements of the grid-interlinked WTGSs are indeed reached by using the previously reported techniques. However, there are some constraints of these approaches [29]–[31], including the complexity of the computational algorithm, long training process, and tremendous efforts exerted in fine-tuning the parameters of the control approach. In addition, these approaches rely on the initial conditions and the solver accuracy.

Adaptive control methodology plays an important role in improving the system responses. In the literature review, various adaptive control schemes were proposed to properly control the WECSs such as adaptive sliding mode control scheme that was utilized to optimize the efficiency of DFIG-based WTGS during the fast disturbances of gusty wind effects [35]. In [36], adaptive fuzzy-logic control strategy was proposed to adjust the dynamic speed control of the VSWT-PMSG in order to improve the system robustness. Moreover, a robust adaptive control strategy is developed to online update the PID controllers' gains for regulating the power of WTGS [37]. In [38], adaptive speed control is presented to achieve the MPPT in small-scale WECS. Furthermore, AFs play a crucial role to solve many problems in different applications, including signal prediction, acoustic echo cancellation, and channel equalization [39]–[43]. Presently, the AFs have been further explored in electric power systems, where affine projection (AP) [13], [44] and CMPN [45], [46] algorithms were applied to on-line adapt the multiple controllers for performance enhancement of RECSs. The performance of these algorithms is evaluated by the computational intricacy features and the convergence rate [44]–[46]. The IMSAF algorithm is considered as one of the latest AF algorithms presented by Yang *et al.* [47]. The main merit of the IMSAF is the ability to achieve the best performance with less computational intricacy over other AF algorithms [47]–[49].

This appears the principle impetus to apply IMSAF algorithm-based self-tuned PI controllers to properly enhance the behavior of the grid-interlinked WTGS.

This article exhibits a new contribution of applying the IMSAF algorithm-based self-tuned PI control approach to enhance the characteristics of the grid-interlinked WTGSs. The proposed IMSAF-based self-tuned PI controller is utilized to adjust the MSC and the GSI through a CCS. The IMSAF algorithm continuously updates the PI controllers' gains in the control strategy for both the converter/inverter without the necessity to optimize or fine-tune. The modeling and control approaches of the system under study are illustrated. To achieve realistic responses, practical wind speed data that captured from Zaafarana wind farm, Egypt, are implemented in this study. The feasibility of the self-tuned or adaptive control scheme is compared with that realized using optimized PI control strategy by the WCA and the GA approaches, considering symmetrical and unsymmetrical faults, as the grid disturbances. The IMSAF algorithm-based self-tuned control scheme is realized to be a precise means for enhancing the behavior of the grid-tied wind generators. According to the authors' knowledge, the IMSAF algorithm-based self-tuned PI control strategy has not been reported till now in the RECS literature.

The article is organized as follows: Section II describes the model of the system. In Section III, the FC control strategy is presented. In Section IV, the proposed IMSAF technology is illustrated. The optimal PI control scheme is discussed in Section V. The simulation analyses and discussion are depicted in Section VI. Finally, Section VII draws the conclusion.

II. MODEL OF THE SYSTEM

Fig. 1 depicts the modelling of the system under study, which is presented to clarify the worthiness of self-tuned PI controllers utilized in controlling the VSCs of the grid-tied VS-WTGS. In this regard, such a system mainly composes of a VSWT, a PMSG, a FC, a dc-link capacitor, a three-phase transformer, and two transmission line circuits. In this study, parameters of the PMSG-based VSWT system are mentioned in Table 1 [13]. The system base power is set 5.0 MVA. The grid-tied VS-WTGS structure is briefly described as follows:

A. WT MODEL

The P_ω captured from the WT is given as [2], [13]:

$$P_\omega = 0.5\rho\pi R^2 V_\omega^3 C_P(\lambda, \beta) \tag{1}$$

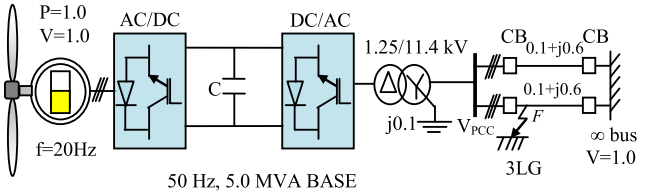

FIGURE 1. Modelling of the system.

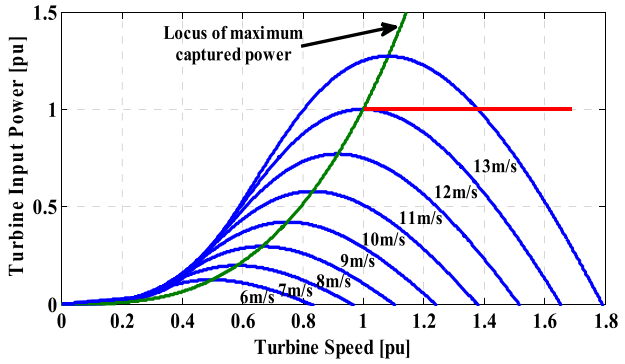

FIGURE 2. WT characteristic with maximum power trajectory.

TABLE 1. Parameters of the PMSG-based VSWT.

PMSG Data			
Rated Power	5.0 [MW]	Stator Resistance	0.01 [pu]
Rated Voltage	1.0 [kV]	d-axis Reactance	1.0 [pu]
Frequency	20 Hz	q-axis Reactance	0.7 [pu]
Number of Poles	150	Field Flux	1.4 [pu]
Inertia Constant	3.0 [s]		
WT Data			
P_{opt}	5.0 [MW]	λ_{opt}	8.1
ρ	1.225 [kg/m^3]	Cut-in V_w	4 [m/s]
R	56 [m]	Rated V_w	12 [m/s]
C_{P-opt}	0.48	Cut-out V_w	25 [m/s]
Gear ratio	1		
DC-link Capacitor Data			
C_{dc}	10 [mF]	V^*_{dc}	2.3 [kV]

The C_P formula is expressed by the following [44]:

$$\lambda = \frac{\omega_r R}{V_w} \tag{2}$$

$$C_P(\lambda, \beta) = \frac{1}{2}\left(\lambda - 0.022\beta^2 - 5.6\right) e^{-0.17\lambda} \tag{3}$$

Characteristic of a VSWT utilized in this investigation is elucidated in Fig. 2, including the maximum power trajectory [13], [20]. Since a rigorous practical recording of wind speed is, commonly, difficult to recognize, it is preferable to obtain the optimum power, P_{opt}, in terms of ω_r as follows [19]:-

$$P_{opt} = 0.5\rho\pi R^2 \left(\frac{\omega_r R}{\lambda_{opt}}\right)^3 C_{P-opt} \tag{4}$$

B. GENERATOR MODEL

The terminal voltages of the PMSG in dq quantities are expressed using the following formulas [2]:-

$$v_{ds} = R_s i_{ds} + L_d \frac{di_{ds}}{dt} - \omega_e L_q i_{qs} \tag{5}$$

$$v_{qs} = R_s i_{qs} + L_q \frac{di_{qs}}{dt} + \omega_e \lambda_m + \omega_e L_d i_{ds} \tag{6}$$

$$\omega_e = P\omega_r \tag{7}$$

The developed torque, T_e, can be written as follows:

$$T_e = \frac{3}{2} P[(L_d - L_q) i_{ds} i_{qs} - \lambda_m i_{qs}] \tag{8}$$

III. FC CONTROL STRATEGY

The concept of a direct-drive PMSG-based VSWT technology, mainly, relies on the utilization a FC. Such a full-capacity FC composes of an MSC, a dc-bus capacitor, and a GSI. The FC control strategy using the IMSAF algorithm-based self-tuned PI controllers is illustrated next.

A. MACHINE-SIDE CONVERTER (MSC)

The MSC is worthy to achieve the maximum power of the WT. A well-known CCS, illustrated in Fig. 3(a), is applied to the MSC. The MSC is linked directly to the generator. So, it can adjust the PMSG active power. The reference real power, P_{opt}, is realized by using the maximum power point tracking approach. On the other hand, I_d adjusts its reactive power, and its reference value, Q^*_{PMSG}, equals zero to perform a unity power operation under steady-state conditions at the PMSG terminals. Note that, four self-tuned or adaptive PI controllers are applied to this work under the cascaded structure. Self-tuned PI-1 and PI-3 controllers are utilized to adjust the reactive and active powers in the outer loops, generating the dq-axes set-point currents, I^*_d and I^*_q. In other words, self-tuned PI-2 and PI-4 are utilized for adjusting the dq-axes currents in the inner loops, generating the set-point

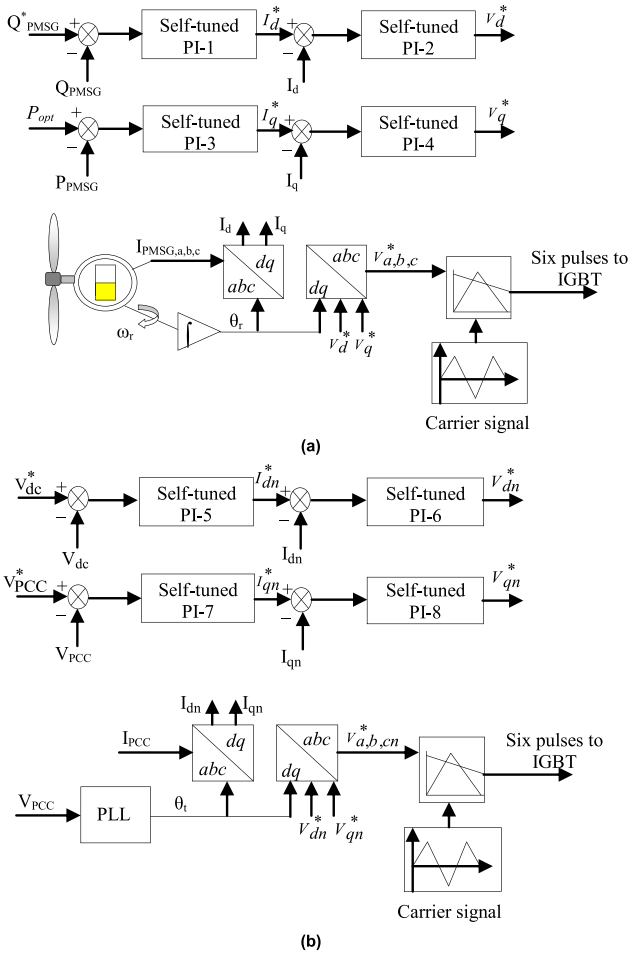

FIGURE 3. Control block diagram. (a) MSC. (b) GSI.

voltage signals, V_{d}^{*} and V_{q}. Then, these signals are converted to their *abc* signals, $V_{a,b,c}^{*}$, using the θ_r that is realized from the ω_r. The $V_{a,b,c}^{*}$ signals are compared with a carrier signal with a triangular shape and its frequency equals 1.0 kHz in order to produce the switching signals of IGBT switches of such MSC.

B. GRID-SIDE INVERTER (GSI)

The GSI, which is essentially a two-level, three-phase, six IGBT switches inverter, is employed to adjust the V_{dc} and the V_{PCC}, at a required value controlled by the operator. Four self-tuned PI controllers through the CCS are applied for this purpose, as illustrated in Fig. 3(b). In such a situation, self-tuned PI-5 and PI-7 controllers are employed to adjust the V_{dc} and V_{PCC} through outer loops, generating the *dq*-axes set-point currents, I_{dn}^{*} and I_{qn}^{*}. The self-tuned PI-6 and PI-8 controllers are employed for controlling the *dq*-axes currents, I_{dn} and I_{qn}. A PLL system is applied to extract the θ_t from the grid voltages. The set-point voltage quantities, V_{dn}^{*} and V_{qn}^{*}, are converted to their set-point waveform, $V_{a,b,cn}^{*}$ using the θ_t. Then, the $V_{a,b,cn}^{*}$ signals are applied to a pulse width modulation technique to produce the gate pulses of electronic switches of such GSI. The self-tuned technique of the PI controllers relies on the IMSAF technology, which is discussed in the next section.

IV. PROPOSED IMSAF TECHNOLOGY

AFs have been employed in various applications. The AF performance is evaluated based on the convergence rate, steady-state error, and computational intricacy characteristics [40]. The LMS and the normalized LMS (NLMS) AF approaches are widely employed because of their features, including the simple implementation, robust performance, and less computational intricacy. However, the LMS algorithms suffer from the weak convergence speed, especially for colored input signals [48], [49]. Therefore, various approaches were presented to expedite the convergence rate of the NLMS algorithm, such as AP and CMPN algorithms. Notably, this enhancement is realized at the cost raised computational intricacy. So, several low computational complexity approaches were proposed. Recently, the conventional MSAF technology is utilized to speed up the convergence rate for input signals having a large spectral dynamic range. While, the IMSAF is proposed to exceed the convergence rate in the radio and colored signals, which require high-order filters to model long acoustic impulse responses. Moreover, the IMSAF algorithm realizes good responses for a highly non-stationary signal in a noisy system [47].

The IMSAF relies on a minimal disturbance concept by nulling the most recent P *posteriori* errors in the N subbands [47]–[49]. This algorithm is derived from the Lagrange multipliers method.

Consider the required signal $d\,(n)$ which appears from a linear model as follows [47]:-

$$d\,(n) = \mathbf{w}_o^T \mathbf{u}(n) + v(n) \tag{9}$$

where $\mathbf{w}_o = [w_0, w_1, \ldots\ldots, w_{L-1}]^T$ denotes the length-L tap-weight vector of the system, $\mathbf{u}\,(n) = [u\,(n)\,, u\,(n-1)\,, \ldots, u\,(n-L+1)]^T$ represents the input signal vector, and $v\,(n)$ stands for the system noise.

The $d\,(n)$ and $u\,(n)$ are divided into N subband signals, $d_i(n)$ and $u_i(n)$, through analysis filters $H_i(z)$. The subband input signals $u_i\,(n)$ are filtered by AF to produce the output signals $y_i\,(n)$. Then, the $d_i\,(n)$ and $u_i\,(n)$ signals are decimated by a factor N to produce $d_{i,D}\,(k)$ and $y_{i,D}\,(k)$. The variables n and k are utilized to clarify the original and decimated sequences. The *a priori* and *a posteriori* decimated subband errors are defined as [47]:-

$$e_{i,D}\,(k) = d_{i,D}\,(k) - \mathbf{w}^T\,(k)\,\mathbf{u}_i\,(k) \tag{10}$$

$$\xi_{i,D}\,(k) = d_{i,D}\,(k) - \mathbf{w}^T\,(k+1)\,\mathbf{u}_i(k) \tag{11}$$

where

$$\mathbf{u}_i\,(k) = [u_i\,(kN)\,, u_i\,(kN-1)\,, \ldots..,u_i\,(kN-M+1)]^T$$

represents the regression vector for the ith subband signal and $\mathbf{w}\,(k) = [w_0\,(k)\,, w_1\,(k)\,, \ldots.,w_{M-1}\,(k)]^T$ is the weight vector of AF. M is the length of the modeling filter.

The MSAF algorithm depends on a minimal disturbance concept by nulling the *posteriori* errors in all N subbands for each iteration, k, as follows:-

$$\begin{aligned} &\min_{\mathbf{w}(k+1)} ||\mathbf{w}\,(k+1) - \mathbf{w}(k)||^2 \\ &\text{subject to } \xi_{i,\mathrm{D}}\,(k) = 0, \quad i = 0,\ 1, \ldots, N-1 \end{aligned} \tag{12}$$

where $||.||^2$ stands for the squared Euclidean norm of a vector.

The IMSAF algorithm is inspired from the AP algorithm, since further recent data is utilized to update the AF. Here, we suggest to null the most recent P *a posteriori* errors in the N subbands, *i.e.*, a total PN error signals, and then

$$\begin{aligned} d_{i,D}\,(k-j) = \mathbf{w}^T\,(k+1)\,\mathbf{u}_i(k-j), \quad & i = 0, 1, \ldots.., N-1; \\ & j = 0, 1, \ldots\ldots.., P-1 \end{aligned} \tag{13}$$

To achieve a merged solution, some quantities are defined as [47]:-

$$\begin{aligned} \mathbf{U}\,(k) = {} & [\mathbf{u}_0\,(k)\,, \ldots., \mathbf{u}_0\,(k-P+1)\,, \mathbf{u}_1\,(k)\,, \\ & \ldots., \mathbf{u}_1\,(k-P+1)\,, \\ & \ldots., \mathbf{u}_{\mathrm{N}-1}\,(k)\,, \ldots.,\mathbf{u}_{N-1}\,(k-P+1)] \end{aligned} \tag{14}$$

$$\begin{aligned} \boldsymbol{d}_{\mathrm{D}}\,(k) = {} & [d_{0,\mathrm{D}}\,(k)\,, \ldots., d_{0,\mathrm{D}}\,(k-P+1)\,, d_{1,\mathrm{D}}\,(k)\,, \\ & \ldots., d_{1,D}\,(k-P+1)\,, \ldots., d_{N-1,D}\,(k)\,, \\ & \ldots\ldots\ldots d_{\mathrm{N}-1,\mathrm{D}}\,(k-P+1)]^T, \end{aligned} \tag{15}$$

$$\begin{aligned} \mathbf{e}_{\mathrm{D}}\,(k) = {} & [e_{0,\mathrm{D}}\,(k)\,, \ldots., e_{0,\mathrm{D}}\,(k-P+1)\,, e_{1,\mathrm{D}}\,(k)\,, \\ & \ldots., e_{1,\mathrm{D}}\,(k-P+1) \ldots., e_{N-1,\mathrm{D}}\,(k)\,, \\ & \ldots\ldots\ldots e_{N-1,\mathrm{D}}\,(k-P+1)]^T \\ = {} & \mathbf{d}_{\mathrm{D}}\,(k)\,\mathbf{U}^T\,(k)\,\mathrm{w}\,(k)\,, \end{aligned} \tag{16}$$

$$\begin{aligned} \boldsymbol{\xi}_D\,(k) = {} & [\xi_{0,D}\,(k)\,, \ldots., \xi_{0,D}\,(k-P+1)\,, \xi_{1,D}\,(k) \\ & \ldots., \xi_{1,D}\,(k-P+1) \ldots., \xi_{N-1,D}\,(k)\,, \\ & \ldots., \xi_{\mathrm{N}-1,\mathrm{D}}\,(k-P+1)]^T \\ = {} & \mathbf{d}_{\mathrm{D}}\,(k)\,\mathbf{U}^T\,(k)\,\mathrm{w}\,(k+1)\,, \end{aligned} \tag{17}$$

where P denotes the projection order.

Constraint conditions of (13) are written as follows [47]:-

$$\mathbf{U}^T(k)\mathrm{w}(k+1) = \mathbf{d}_\mathrm{D}(k) \tag{18}$$

We seek $w\,(k+1)$ to solve the constraint optimization criterion by the following:-

$$\underset{\mathbf{w}(k+1)}{min}\ ||\mathbf{w}\,(k+1) - \mathrm{w}\,(k)||^2 \quad \text{subject to } \xi_\mathrm{D}\,(k) = 0 \tag{19}$$

where $\mathbf{0}$ represents the NP X 1 null matrix.

Lagrange multiplier approach is used to resolve the constraint minimization problem. The cost function is expressed as:-

$$J\,[\mathbf{w}\,(k+1)] = \frac{1}{2}\,||\mathbf{w}\,(k+1) - \mathbf{w}\,(k)||^2 + \boldsymbol{\lambda}^T \xi_D\,(k) \tag{20}$$

where $\lambda = [\lambda_0, \lambda_1, \ldots, \lambda_{NP-1}]^\mathrm{T}$ denotes the Lagrange multiplier vector. Take the derivative of (20) related to $\mathbf{w}\,(k+1)$ and set it to zero, then

$$\mathbf{w}\,(k+1) = \mathbf{w}\,(k) + \mathbf{U}\,(k)\,\boldsymbol{\lambda} \tag{21}$$

Substituting (21) into (18) and using (16), one has

$$\mathbf{U}^T\,(k)\,\mathbf{U}\,(k)\,\lambda = \mathbf{e}_\mathrm{D}\,(k) \tag{22}$$

Solve λ from (22) and substitute it into (21), a recursive relation is presented for updating the tap-weight vector as;

$$\mathbf{w}(k+1) = \mathbf{w}(k) + \mu\mathbf{U}(k)[\mathbf{U}^T(k)\mathbf{U}(k)]^{(-1)}\mathrm{e}_\mathrm{D}(k) \tag{23}$$

To prevent the numerical instability, a regularization parameter ε is added to the diagonal elements of $\mathbf{U}^T\,(k)\,\mathbf{U}\,(k)$. Therefore, a more practical update equation of the IMSAF algorithm can be expressed as follows:-

$$\mathbf{w}\,(k+1) = \mathbf{w}\,(k) + \mu\mathbf{U}\,(k)\,[\mathbf{U}^T\,(k)\,\mathbf{U}\,(k) + \varepsilon\mathbf{I}]^{-1}\mathbf{e}_\mathrm{D}\,(k) \tag{24}$$

where $\mathbf{I}$ stands for the identity matrix with size NP X NP and μ is the step size that is considered in the range of $0 < \mu \leq 2$ to minimize the error signal with rapid convergence.

The IMSAF keeps the next coefficient vector $\mathbf{w}\,(k+1)$ as close to the $\mathbf{w}\,(k)$, and forcing the *posterior* errors to zero.

In this work, the IMSAF algorithm is applied to on-line update the proportional and integral gains of all PI controllers under the CCS for both the converter/inverter. The on-line adaptation of the PI controller gains basically relies on (24). The update of the PI controllers' gains is represented using the next equations:

$$k_p(k+1) = k_p(k) + \Delta k_p(k) \tag{25}$$

$$k_i(k+1) = k_i(k) + \Delta k_i(k) \tag{26}$$

By comparing (24) with (25)-(26), the change of the controller gains ($\Delta k_p\,(k)$ and $\Delta k_i\,(k)$) is realized as:

$$\Delta k_p\,(k) = \Delta k_i\,(k) = \mu U\,(k)\,[U^T\,(k)\,U\,(k) + \varepsilon I]^{-1} e_D\,(k) \tag{27}$$

From Eqs. (25)-(27), the IMSAF algorithm is implemented in this study by considering the input vector $\mathbf{U}\,(k)$ equals $[m\,(k-1)\,, e\,(k)\,-e\,(k-1)\,, e\,(k)\,+e\,(k+1)]^T$, where $m\,(k-1)$ denotes one-step previous output of the PI controller. The present coefficient vector $\mathbf{w}(k) = [1, k_p, k_i]^T$. Fig. 4 depicts the control scheme of the IMSAF-based self-tuned PI control approach. The difference between the set-point signal ($U^*\,(k)$) and the actual signal ($U(k)$) represents the error signal $\boldsymbol{e}\,(k)$. These two input signals to the summing point are changed related to the location of the self-tuned PI controller in the control approach. All the self-tuned PI controllers presented in Figs. 3(a)-(b) are on-line updated using the proposed IMSAF algorithm, as clarified in Fig. 4. For an instant, for self-tuned PI-3 controller indicated in Fig. 3(a), $U^*\,(k)$ and $U\,(k)$ are P_{opt} and P_{PMSG}, and the controller output $m\,(k)$ denotes the current I_q^*.

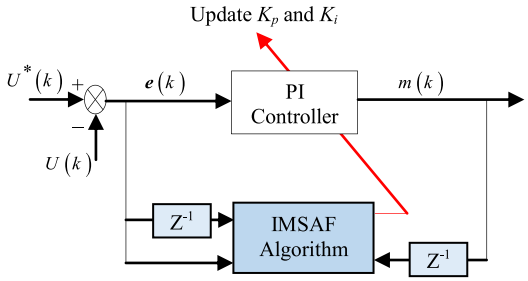

FIGURE 4. Self-tuned PI controller based on IMSAF algorithm.

V. OPTIMAL PI CONTROL SCHEME

To confirm the efficacy of the VS-WTGS interlinked to the electric network under several operating cases, the simulation analyses of the system under study using the IMSAF-based self-tuned PI control approach is compared with that obtained using the PI control scheme optimized by the WCA and the GA approaches. Four PI controllers optimized by the WCA and the GAs approach are utilized in the CCS for each converter/inverter. The WCA and GAs approaches are employed to properly fine-tune the eight PI controllers as follows.

A. THE OPTIMIZATION ALGORITHMS

1) GAs APPROACH

The GAs approach-based evolutionary algorithm is a robust optimization technique applied to get the best solutions of optimization problems in several engineering applications [2], [27]. The heuristic search of GA relies on the survival of the fittest [50]. In the GA, the optimization process is started with a random generation of the population. The population is composed of a group of chromosomes. The solution that performed for each string can be assessed when the random population is realized. The function applied for assessing the solution for each step is known as the fitness function. The GA applies inspired methods, such as natural selection, reproduction, mutation, and crossover [2], [50].

Here, the optimization selection approach depends on uniform selection technique, in which the response is obtained with no bias and minimal spread [2].

2) WCA APPROACH

The WCA is a new meta-heuristic optimization approach, which was introduced in 2012 [51]. The WCA was inspired by the water cycle process in nature. This cycle is depicted as follows; the water branches are gathered to establish a river, which terminates to the sea. Then, the water in rivers is vaporized due to the weather conditions producing clouds in the sky. Finally, the clouds are condensed and return back to the earth in the rains form in the winter season [31], [51]. The merits of the WCA are the fast convergence speed and the lower parameters to be fine-tuned. The WCA were efficiently applied to solve various optimization problems in different applications such as designing the optimal control strategy for efficient operation of microgrids [31] and for wave energy conversion systems [17], load frequency control of interconnected power systems [52], and optimal dealing with the overcurrent relays coordination problems in electric power systems [53]. The detailed WCA is mentioned in [31].

B. THE OPTIMIZATION STEPS

In this study, the GAs and WCA approaches are presented to design the PI controllers' gains. The design methodology of the optimal PI control scheme using the GAs and WCA approaches is performed as the next:

STEP 1) VARIABLES SELECTION:

The PI controllers' parameters are chosen as the design variables, where the X_1, X_3,……, and X_{15}, respectively, denote the proportional gains (k_p) of PI-1, PI-2,……., and PI-8. X_2, X_4,…, and X_{16}, respectively, denote the integral gains (k_i) of PI-1, PI-2,……., and PI-8.

STEP 2) CREATION OF OBJECTIVE FUNCTION:

The system modeling of the grid-tied VS-WTGS controlled by the optimized PI control strategy is set up. The GAs and WCA approaches are applied to minimize the objective function using the following steps:-

a: FOR MSC CONTROL SCHEME

In the inner loop, the transfer function (TF) of I_q in S-domain form is given as:

$$NM = \frac{I_q^*}{I_q} = \frac{\left(X_7 + \frac{X_8}{S}\right) * (1/\,(R_s + L_s * S)}{1 + \left(X_7 + \frac{X_8}{S}\right) * \left(\frac{1}{R_s + L_s * S}\right)} \tag{28}$$

where (I_q^* and I_q) are, respectively, the set-point and actual q-axis currents, and (X_7 and X_8) denote the gains of PI-4.

Besides, in the outer loop, the TF of q-axis control is also represented in S-domain as:

$$\frac{P_{opt}}{P_{pmsg}} = \frac{\left(X_5 + \frac{X_6}{S}\right) * \frac{1.5 P \lambda_m^2 V_w}{R} * NM}{1 + \left(X_5 + \frac{X_6}{S}\right) * \frac{1.5 P \lambda_m^2 V_w}{R} * NM} \tag{29}$$

where (X_5 and X_6) stand for the gains of PI-3.

For a simple design, the I_d and I_q controllers have the same dynamics. Therefore, the proper design of the PI gains is done only for the I_d control.

b: FOR GSI CONTROL SCHEME

In the inner loop, the TF of I_{dn} is represented in the S-domain form as follows:

$$KL = \frac{I_{dn}^*}{I_{dn}} = \frac{\left(X_{11} + \frac{X_{12}}{S}\right) * (1/(R_g + L_g * S)}{1 + \left(X_{11} + \frac{X_{12}}{S}\right) * \left(\frac{1}{R_g + L_g * S}\right)} \tag{30}$$

where (I_{dn}^* and I_{dn}) stand for the set-point and actual grid d-axis currents, (R_g and L_g) denote the resistance and inductance of the network, and (X_{11} and X_{12}) stand for the gains of PI-6.

Also, in the outer loop, the TF of dn-axis control in the S-domain form is written as:

$$\frac{V_{dc}^*}{V_{dc}} = \frac{\left(X_9 + \frac{X_{10}}{S}\right) * \frac{1}{C_{dc} S} * KL}{1 + \left(X_9 + \frac{X_{10}}{S}\right) * \frac{1}{C_{dc} S} * KL} \tag{31}$$

where (X_9 and X_{10}) are the gains of PI-5.

For simplicity, the TF of I_{qn} in inner-loop is the same to (30). Thus, the Eqs. (28) to (31) are linearized in state-space system, where the matrix A that relates to the poles of the closed-loop control can be realized. The objective function, J, is given as [54]:

$$J = \frac{1}{\left|\underset{i=1,2,3.....}{max\{Re(\lambda_i)\}}\right|} + Z_b$$
$$Z_b = \begin{cases} 1000, & if \;\; \max\{Re\,(\lambda_i)\} \geq 0 \\ 0 & otherwise \end{cases} \tag{32}$$

where λ_i denotes the ith mode eigenvalue of the matrix A, and (Z_b) is a function used to achieve a stable system [54]. The system stability is determined based on the real part of the eigenvalues. Therefore, should be greater for avoiding the system instability.

STEP 3) APPLICATION OF OPTIMIZATION TECHNIQUES:

The GAs and WCA approaches are performed directly in (32) for minimizing the function, J, and obtain the optimal gains of PI controllers, which are clarified in Table 2. Here, the MATLAB toolbox for the GA technique is used [55]. Characteristics of the GA and WCA are indicated in [27] and [31], respectively. The optimization approaches are terminated with the average change in the fitness value was $\leq$ 1e−7. Fig. 5 indicates the fitness function convergence of the GA and WCA approaches.

VI. SIMULATION ANALYSES AND DISCUSSION

A complete model of a grid-tied VS-WTGS is introduced. The simulation results are performed using the MATLAB/Simulink software [55]. The time step is chosen 20 μs. The simulation time is selected related to the scenario type. Different scenarios are implemented through this study to

TABLE 2. Optimal values of PI controllers' gains.

Algorithm	PI no.	K_p	K_i
GAs	PI-1	9.213	4.0931
	PI-2	3.486	0.312
	PI-3	8.452	3.542
	PI-4	4.486	1.312
	PI-5	3.245	1.378
	PI-6	4.512	2.371
	PI-7	4.682	1.826
	PI-8	3.512	2.371
WCA	PI-1	8.301	3.984
	PI-2	3.148	0.432
	PI-3	7.617	3.715
	PI-4	4.718	1.278
	PI-5	4.018	1.438
	PI-6	4.189	2.479
	PI-7	5.184	1.974
	PI-8	3.471	2.149

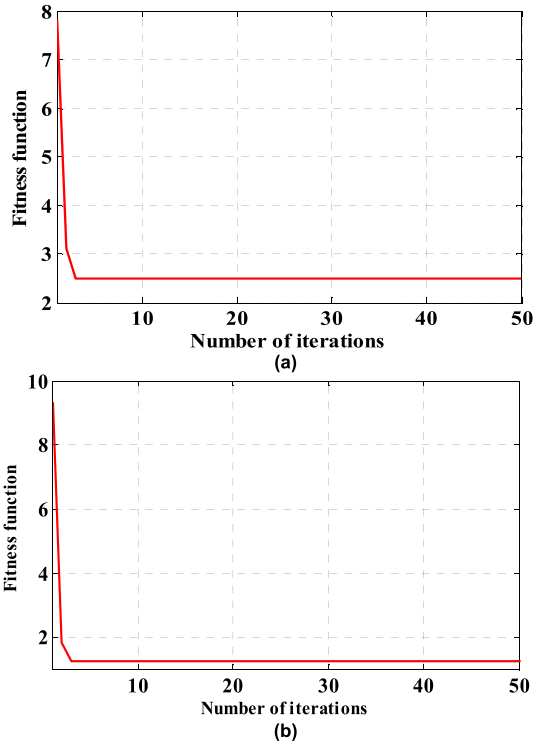

FIGURE 5. Fitness convergence. (a) GA. (b) WCA.

confirm the validity of the grid-tied WTGS model and the efficacy of the IMSAF-based self-tuned PI control strategy, as elucidated next.

A. TRANSIENT CHARACTERISTIC ANALYSIS

This scenario aims at evaluating the efficacy of the IMSAF algorithm-based self-tuned control approach for enhancing the transient stability response of the grid-interlinked PMSG-based VSWT. To confirm this validity, the simulation analyses of the self-tuned control approach is compared with that realized when the GA and WCA-based PI controllers are used, considering subjecting the system to different fault conditions. The symmetrical 3-line-to-ground (3LG) fault occurs at the fault point F of the grid-tied WTGS, as indicated in Fig. 1. The disturbance is supposed to be a temporary fault with duration of 1.0 s. The circuit breakers (CBs) take the action to disconnect the faulted line at t = 1.1 s. At the instant (t=1.5 s), the CBs are successfully reclosed again. In this analysis, the wind speed is considered constant at its rated speed of 12 m/s. This is due to it is regarded that the wind speed does not vary dramatically through the short period of the simulation for this analysis. During the network disturbance, the V_{PCC} drops suddenly from its rated value of 1.0 pu and the GSI has to inject a suitable amount of reactive power in order to help the V_{PCC} to successfully return to the pre-fault value, as pointed out in Fig. 6(a). It can be mentioned that the V_{PCC} profile using the IMSAF-based self-tuned PI controller is better damped with lower oscillations over that realized using the optimized PI controller by the GA and WCA approaches. Fig. 6(b) clarifies the response of the PMSG rotor speed using both control strategies. Note that, the PMSG runs at its rated ω_r of 1.0 pu and the operator allows $\pm$ 5% of this speed as the maximum/minimum speed that higher/lower the rated ω_r before discounting from the grid. In addition, the IMSAF-based self-tuned PI controller can efficiently help the generator speed to realize its original value quickly over the optimized PI control scheme. Fig. 6(c) clarifies the P_{PCC} response. Notably, the IMSAF-based self-tuned PI control strategy can efficiently adjust the maximum power delivered to the power grid and attain an excellent response in comparison with the GA and WCA-based PI control schemes. Fig. 6(d) indicates the reactive power response, Q_{PCC}, using both control approaches. It is worthy of noting that the Q_{PCC} profile has a better damped with minimum fluctuation and becomes more enhanced than that realized using the GA and WCA-based PI control schemes. Fig. 6(e) depicts the V_{dc} response. Note that, an OVPS that utilizes a breaking chopper [27], is regarded in this analysis so as to attain the V_{dc} response in an acceptable range during the fault condition. It is clearly observed that without using the dc-bus OVPS, the V_{dc} raises rapidly at the instant of the fault, leading to unstable operation of the FC. Moreover, it is pointed out that the proposed self-tuned control approach achieves a very fast response with minimal oscillations over that of the optimized PI controller by the GA and WCA approaches. The transient performance specifications, such as the E_{ss}, M_{os}/M_{us}, and T_s using both strategies are clarified in Table 3. Notably, the transient performance specifications using the IMSAF-based self-tuned PI control approach are lower than that realized when the GA and WCA-based optimal PI controllers are used.

Furthermore, a fair comparison is carried out for the VS-WTGS interlinked to the electric network using the IMSAF-based self-tuned PI control scheme and the optimized PI controllers by the GA and WCA approaches under different unsymmetrical fault conditions, such as 2-line-to-ground (2LG), line-to-line (LL), and 1-line-to-ground (1LG) fault conditions. The V_{PCC} response using

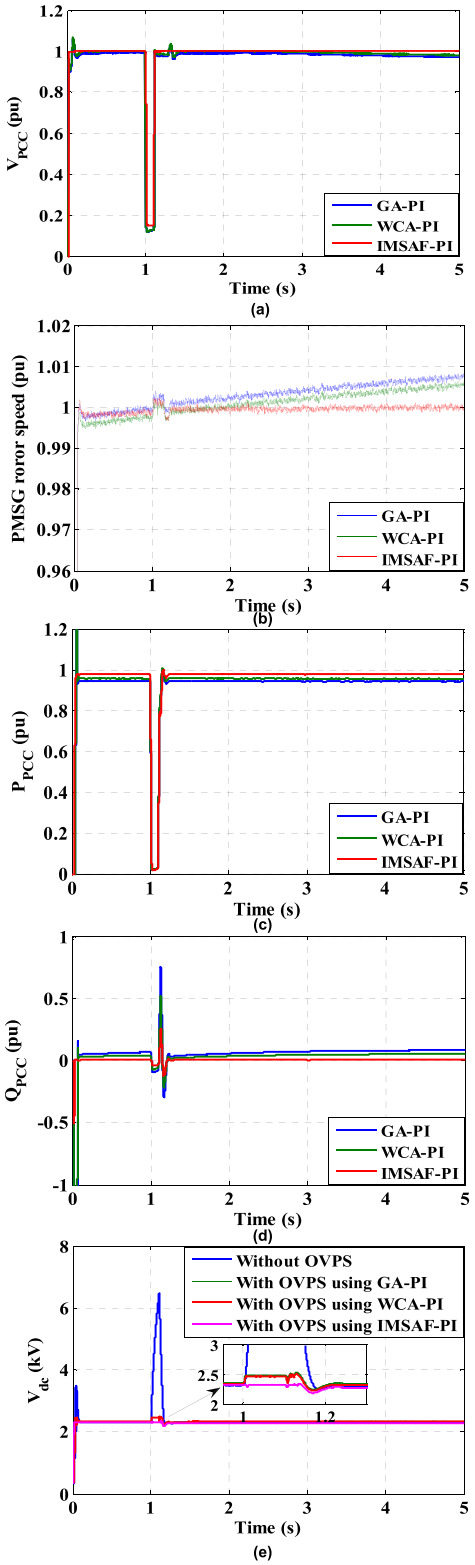

FIGURE 6. Performances under symmetrical 3LG fault. (a) V_{PCC}. (b) PMSG rotor speed. (c) P_{PCC}. (d) Q_{PCC}. (e) V_{dc}.

these fault situations is depicted Figs. 7(a)-(c). It is clearly noticed that the V_{PCC} profile with the proposed self-tuned control approach achieves much better damped response with

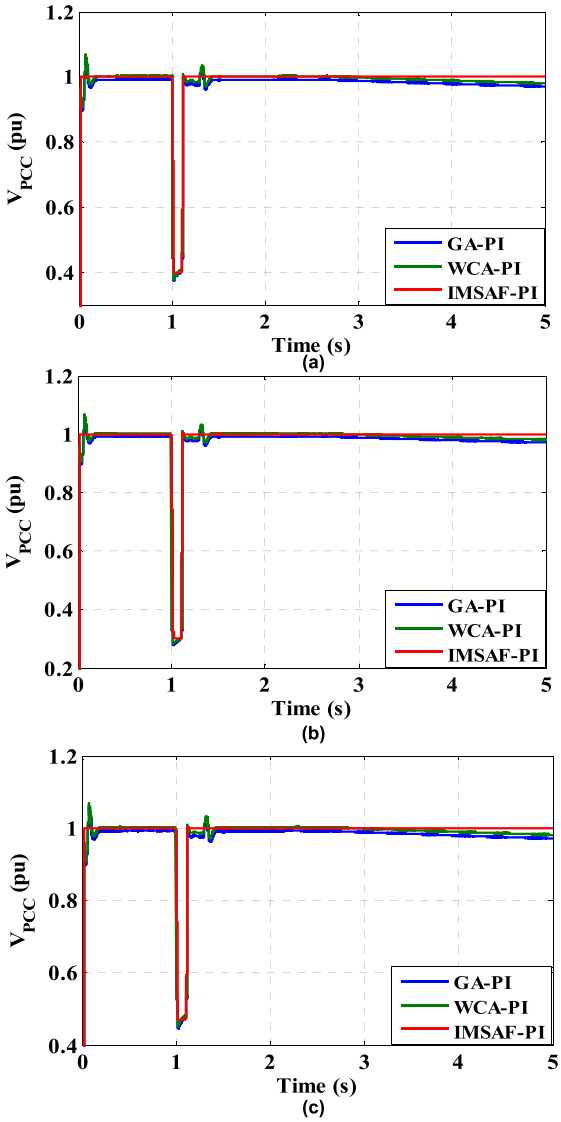

FIGURE 7. VPCC performance under unsymmetrical faults. (a) 2LG fault. (b) LL fault. (c) 1LG fault.

lower oscillations over that realized using the optimized PI controller by the GA and WCA approaches.

Notably, the transient stability responses are rigorously enhanced with the help of using the IMSAF-based adaptive PI control approach over that achieved when the GA and WCA-based PI controller are used. The proposed control strategy has a capability of returning these performances to their pre-fault values after the disturbance removal.

B. DYNAMIC CHARACTERISTIC ANALYSIS

For achieving precise performances, the dynamic behavior of the grid-tied WTGS using the IMSAF-based self-tuned PI controller is assessed by applying practical wind speed data that captured from Zaafarana wind farm, Egypt, on 24 September 2018. The simulation studies using the proposed self-tuned control strategy are compared with that achieved using the optimized PI controller by the GA

TABLE 3. Transient performance specifications.

System response	Specification	GA-PI	WCA-PI	IMSAF-PI
V_{PCC}	E_{ss} (pu)	0.03	0.02	0
	M_{us} (%)	88	86	84
	T_s (s)	1.43	1.2	1.0
Rotor speed of PMSG	E_{ss} (pu)	0.02	0.01	0
	M_{os} (%)	0.6	0.4	0.2
	T_s (s)	8	6	1.2
P_{PCC}	E_{ss} (pu)	0.09	0.06	0.02
	M_{us} (%)	97.9	96	94
	T_s (s)	1.37	1.2	1.1
Q_{PCC}	E_{ss} (pu)	0.073	0.053	0.002
	M_{os} (%)	74.8	68.3	28
	T_s (s)	9.3	8.2	1.1
V_{dc}	E_{ss} (pu)	0.04	0.03	0.002
	M_{os} (%)	7.7	5.9	0.3
	T_s (s)	1.14	1.11	1.0

approach. These analyses are done using MATLAB/Simulink program from 12.10 to 12.15 pm. Fig. 8(a) points out the wind speed pattern of this wind power plant. It can be noted that within the five minutes pattern, the wind speed varies from 9.3 to 12.96 m/s to clarify a wide range of wind speed fluctuation. Fig. 8(b) points out the performance of the PMSG rotor speed, which guarantees its operation through various operating regions. Moreover, the PMSG speed becomes more stable and accurately realizes its rated value using the IMSAF-based PI controller over that of the optimized PI control scheme. Note that, during the high wind speeds, a blade pitch controller that is reported in [19], is taken into account in this study to remain the PMSG speed constant. The P_{PCC} response is plotted using both control strategies, as depicted in Fig. 8(c). It is clearly observed that the P_{PCC} is nearly close to the rated value using the proposed self-tuned technology compared to that of the GA-based optimal control scheme. Fig. 8(d) clarifies the Q_{PCC} profile, which is controlled using the GSI to consequently maintain the V_{PCC} constant. It can be noted here that the Q_{PCC} profile using the IMSAF technology has better damped, faster, and much better enhanced performance over that realized when the GA-based PI control strategy is used. Fig. 8(e) demonstrates the V_{PCC} response. It is noticeable that the V_{PCC} can realize the rated value precisely with lower overshoot and oscillations with the help of using the self-tuned control approach compared with the GA-based PI controller. The V_{dc} profile is pointed out in Fig. 8(f). It is seen that in spite of the wind speed fluctuations, the V_{dc} profile has small fluctuations and better enhanced performance using the IMSAF-based PI control approach over the GA-based optimal control scheme.

From these results, it is noticed that the IMSAF-based self-tuned PI control approach can capture the maximum power from the WT and transfer it to the power network under various operating situations even through the deep and sharp wind speed variations. Moreover, with the self-tuned technology, the V_{dc} and the V_{PCC} are maintained constant during the wind speed fluctuations. Notably, the IMSAF-based self-tuned PI control approach achieves much better-damped response, such as faster with minimum ripples, lower M_{os}/M_{us}, lower

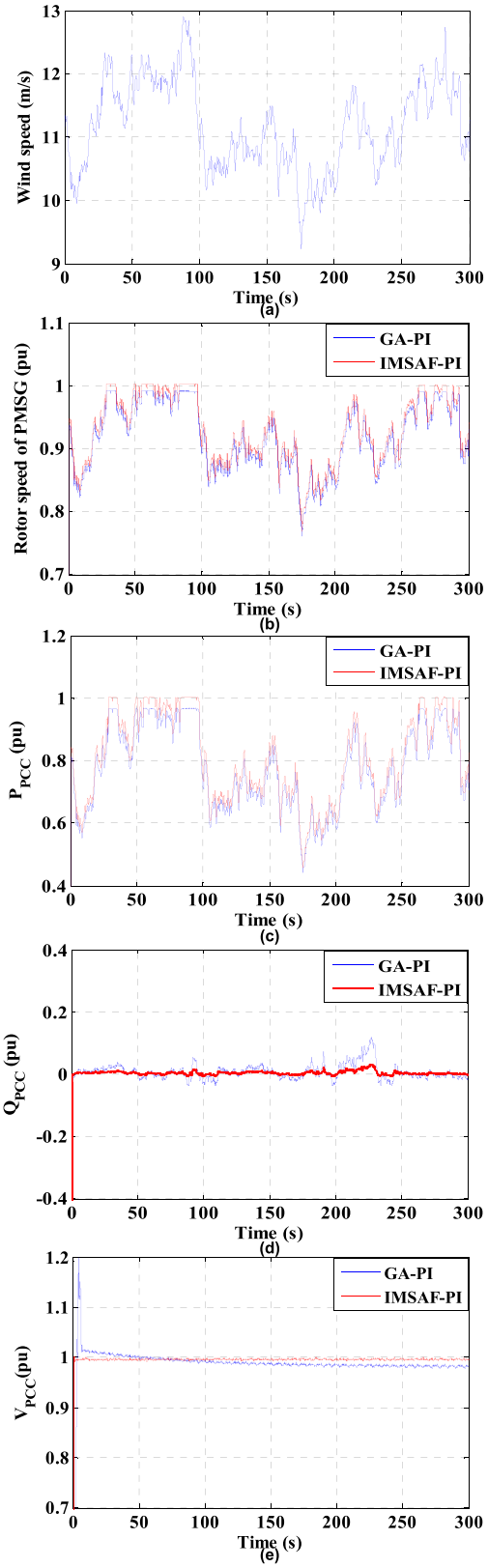

FIGURE 8. Performances using practical wind speed data. (a) Wind speed. (b) PMSG rotor speed. (c) P_{PCC}. (d) Q_{PCC}. (e) V_{PCC}. (f) V_{dc}.

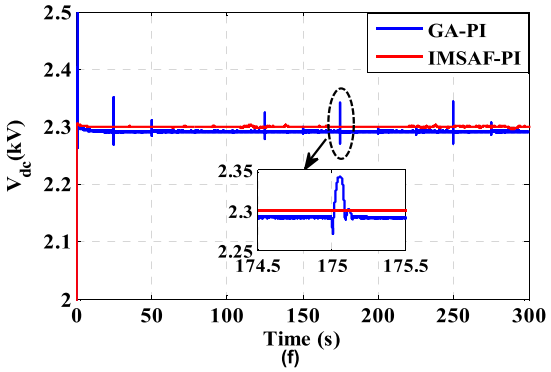

FIGURE 8. ***(Continued)*** **Performances using practical wind speed data. (a) Wind speed. (b) PMSG rotor speed. (c) P_{PCC}. (d) Q_{PCC}. (e) V_{PCC}. (f) V_{dc}.**

T_s, and lower E_{ss} than that obtained when the optimized PI controllers by the GA are used. The high response, precision, and distinction of the proposed self-tuned control strategy reflect the precise design and robustness of the IMSAF to minimize the error signals, achieving rigorous and satisfactory responses compared with the GA-based optimal PI control scheme.

VII. CONCLUSION

This article has exhibited a new self-tuned PI control approach based on the IMSAF technology so as to improve the behavior of the VS-WTGS interconnected to the power grid. Cascaded self-tuned PI controllers were developed to effectively adjust both of the MSC and the GSI. The IMSAF technology distinguishes by its rapid response, which was applied to on-line update the proportional and integral gains of the multiple PI controllers in an expedited way. The proposed self-tuned control strategy pointed out competitive features and good potentials to deal with heavy nonlinear systems, especially for the RECSs. Various scenarios were promoted to confirm the efficacy of the proposed self-tuned control approach. With the IMSAF, the PMSG-based VS-WTGS system has achieved lower values of the transient responses over that obtained using the GA and the WCA. The E_{ss} of the V_{PCC} profile using IMSAF was decreased by 100% over that of using both optimization approaches. Moreover, the M_{os} of the Q_{PCC} response using IMSAF was decreased by 62.5% and 59% than that by using the GA and WCA approaches. Furthermore, the T_s response of the PMSG rotor speed profile was decreased by 85% and 80% over that by using the GA and the WCA, respectively. From the simulation studies, it can be claimed that the transient and dynamic performances using the self-tuned control approach are faster, better damped with lower fluctuations, and superior to that realized using the optimized PI controller by the GA and WCA approaches, taking into account various network fault conditions. The main objective of using the IMSAF technology is that the control system no longer needs intricacy approaches to properly design the multiple PI controllers. Notably, the proposed adaptive technology is not limited to the control of the VS-WTGS. Future work will concentrate on expanding the proposed IMSAF technology-based adaptive fuzzy logic control strategy to adjust the power system applications, energy storage devices, and smart grids, achieving excellent responses in the RECSs.

REFERENCES

[1] Global Wind Energy Council (GWEC). *Annual Market Update 2018, Global Wind Report*. [Online]. Available: http://www.gwec.net

[2] M. H. Qais, H. M. Hasanien, and S. Alghuwainem, "A grey wolf optimizer for optimum parameters of multiple PI controllers of a grid-connected PMSG driven by variable speed wind turbine," *IEEE Access*, vol. 6, pp. 44120–44128, 2018.

[3] X. Zeng, J. Yao, Z. Chen, W. Hu, Z. Chen, and T. Zhou, "Co-ordinated control strategy for hybrid wind farms with PMSG and FSIG under unbalanced grid voltage condition," *IEEE Trans. Sustain. Energy*, vol. 7, no. 3, pp. 1100–1110, Jul. 2016.

[4] H. Chen, D. Xu, and X. Deng, "Control for power converter of small-scale switched reluctance wind power generator," *IEEE Trans. Ind. Electron.*, early access, Mar. 11, 2020, doi: 10.1109/TIE.2020.2978689.

[5] M. M. Namazi, S. M. S. Nejad, A. Tabesh, A. Rashidi, and M. Liserre, "Passivity-based control of switched reluctance-based wind system supplying constant power load," *IEEE Trans. Ind. Electron.*, vol. 65, no. 12, pp. 9550–9560, Dec. 2018.

[6] T. M. Masaud and P. K. Sen, "Modeling and analysis of self-excited induction generator for wind energy conversion," in *Proc. IEEE Power Energy Soc. Innov. Smart Grid Technol. Conf. (ISGT)*, Feb. 2015, pp. 1–5, doi: 10.1109/ISGT.2015.7131901.

[7] V. Nayanar, N. Kumaresan, and N. Ammasai Gounden, "A Single-Sensor-Based MPPT controller for wind-driven induction generators supplying DC microgrid," *IEEE Trans. Power Electron.*, vol. 31, no. 2, pp. 1161–1172, Feb. 2016.

[8] N. K. Swami Naidu and B. Singh, "Doubly fed induction generator for wind energy conversion systems with integrated active filter capabilities," *IEEE Trans. Ind. Informat.*, vol. 11, no. 4, pp. 923–933, Aug. 2015.

[9] M. Ammar and M. E. Ammar, "Enhanced flicker mitigation in DFIG-based distributed generation of wind power," *IEEE Trans. Ind. Informat.*, vol. 12, no. 6, pp. 2041–2049, Dec. 2016.

[10] K. Shi, X. Yin, L. Jiang, Y. Liu, Y. Hu, and H. Wen, "Perturbation estimation based nonlinear adaptive power decoupling control for DFIG wind turbine," *IEEE Trans. Power Electron.*, vol. 35, no. 1, pp. 319–333, Jan. 2020.

[11] R. Basak, G. Bhuvaneswari, and R. R. Pillai, "Low-voltage ride-through of a synchronous generator-based variable speed grid-interfaced wind energy conversion system," *IEEE Trans. Ind. Appl.*, vol. 56, no. 1, pp. 752–762, Jan. 2020.

[12] W. Gul, Q. Gao, and W. Lenwari, "Optimal design of a 5-MW double-stator single-rotor PMSG for offshore direct drive wind turbines," *IEEE Trans. Ind. Appl.*, vol. 56, no. 1, pp. 216–225, Jan. 2020.

[13] H. M. Hasanien and S. M. Muyeen, "Affine projection algorithm based adaptive control scheme for operation of variable-speed wind generator," *IET Gener., Transmiss. Distrib.*, vol. 9, no. 16, pp. 2611–2616, Dec. 2015.

[14] J.-S. Lee and K.-B. Lee, "Open-circuit fault-tolerant control for outer switches of three-level rectifiers in wind turbine systems," *IEEE Trans. Power Electron.*, vol. 31, no. 5, pp. 3806–3815, May 2016.

[15] R. Pena-Alzola, D. Campos-Gaona, P. F. Ksiazek, and M. Ordonez, "DC-link control filtering options for torque ripple reduction in low-power wind turbines," *IEEE Trans. Power Electron.*, vol. 32, no. 6, pp. 4812–4826, Jun. 2017.

[16] H. M. Hasanien, "Shuffled frog leaping algorithm-based static synchronous compensator for transient stability improvement of a grid-connected wind farm," *IET Renew. Power Gener.*, vol. 8, no. 6, pp. 722–730, Aug. 2014.

[17] H. M. Hasanien, "Transient stability augmentation of a wave energy conversion system using a water cycle algorithm-based multiobjective optimal control strategy," *IEEE Trans. Ind. Informat.*, vol. 15, no. 6, pp. 3411–3419, Jun. 2019.

[18] K. Ogata, *Modern Control Engineering*. 5th ed. Upper Saddle River, NJ, USA: Prentice-Hall, 2018.

[19] S. M. Muyeen, R. Takahashi, T. Murata, and J. Tamura, "Integration of an energy capacitor system with a variable-speed wind generator," *IEEE Trans. Energy Convers.*, vol. 24, no. 3, pp. 740–749, Sep. 2009.

[20] S. M. Muyeen, R. Takahashi, and J. Tamura, "Operation and control of HVDC-connected offshore wind farm," *IEEE Trans. Sustain. Energy*, vol. 1, no. 1, pp. 30–37, Apr. 2010.
[21] S. M. Muyeen, "A combined approach of using an SDBR and a STATCOM to enhance the stability of a wind farm," *IEEE Syst. J.*, vol. 9, no. 3, pp. 922–932, Sep. 2015.
[22] M. Alberdi, M. Amundarain, A. J. Garrido, I. Garrido, O. Casquero, and M. De la Sen, "Complementary control of oscillating water column-based wave energy conversion plants to improve the instantaneous power output," *IEEE Trans. Energy Convers.*, vol. 26, no. 4, pp. 1021–1032, Dec. 2011.
[23] M. S. El Moursi, J. L. Kirtley, and W. Xiao, "Fault ride through capability for grid interfacing large scale PV power plants," *IET Gener., Transmiss. Distrib.*, vol. 7, no. 9, pp. 1027–1036, Sep. 2013.
[24] K. Kawabe and K. Tanaka, "Impact of dynamic behavior of photovoltaic power generation systems on short-term voltage stability," *IEEE Trans. Power Syst.*, vol. 30, no. 6, pp. 3416–3424, Nov. 2015.
[25] F. Islam, H. Hasanien, A. Al-Durra, and S. M. Muyeen, "A new control strategy for smoothing of wind farm output using short-term ahead wind speed prediction and flywheel energy storage system," in *Proc. Amer. Control Conf. (ACC)*, Jun. 2012, pp. 3026–3031.
[26] G. Islam, S. M. Muyeen, A. Al-Durra, and H. M. Hasanien, "RTDS implementation of an improved sliding mode based inverter controller for PV system," *ISA Trans.*, vol. 62, pp. 50–59, May 2016.
[27] H. M. Hasanien and S. M. Muyeen, "Design optimization of controller parameters used in variable speed wind energy conversion system by genetic algorithms," *IEEE Trans. Sustain. Energy*, vol. 3, no. 2, pp. 200–208, Apr. 2012.
[28] M. N. Ambia, H. M. Hasanien, A. Al-Durra, and S. M. Muyeen, "Harmony search algorithm-based controller parameters optimization for a distributed-generation system," *IEEE Trans. Power Del.*, vol. 30, no. 1, pp. 246–255, Feb. 2015.
[29] H. M. Hasanien, "Performance improvement of photovoltaic power systems using an optimal control strategy based on whale optimization algorithm," *Electr. Power Syst. Res.*, vol. 157, pp. 168–176, Apr. 2018.
[30] H. M. Hasanien, "Gravitational search algorithm-based optimal control of archimedes wave swing-based wave energy conversion system supplying a DC microgrid under uncertain dynamics," *IET Renew. Power Gener.*, vol. 11, no. 6, pp. 763–770, May 2017.
[31] M. Hany Hasanien and M. Matar, "Water cycle algorithm-based optimal control strategy for efficient operation of an autonomous microgrid," *IET Gener., Transmiss. Distrib.*, vol. 12, no. 21, pp. 5739–5746, Nov. 2018.
[32] R. Kumar and N. Sinha, "Modeling and control of dish-stirling solar thermal integrated with PMDC generator optimized by meta-heuristic approach," *IEEE Access*, vol. 8, pp. 26343–26355, 2020.
[33] A. K. Barik and D. C. Das, "Coordinated regulation of voltage and load frequency in demand response supported biorenewable cogeneration–based isolated hybrid microgrid with quasi–oppositional selfish herd optimisation," *Int. Trans. Electr. Energy Syst.*, vol. 30, no. 1, pp. 1–22, Jan. 2020.
[34] A. K. Barik and D. C. Das, "Proficient load-frequency regulation of demand response supported bio-renewable cogeneration based hybrid microgrids with quasi-oppositional selfish-herd optimisation," *IET Gener., Transmiss. Distrib.*, vol. 13, no. 13, pp. 2889–2898, Jul. 2019.
[35] C. A. Evangelista, A. Pisano, P. Puleston, and E. Usai, "Receding horizon adaptive second-order sliding mode control for doubly-fed induction generator based wind turbine," *IEEE Trans. Control Syst. Technol.*, vol. 25, no. 1, pp. 73–84, Jan. 2017.
[36] J. Chen, J. Chen, and C. Gong, "New overall power control strategy for variable-speed fixed-pitch wind turbines within the whole wind velocity range," *IEEE Trans. Ind. Electron.*, vol. 60, no. 7, pp. 2652–2660, Jul. 2013.
[37] H. Habibi, H. Rahimi Nohooji, and I. Howard, "Adaptive PID control of wind turbines for power regulation with unknown control direction and actuator faults," *IEEE Access*, vol. 6, pp. 37464–37479, 2018.
[38] H. Zhao, Q. Wu, C. N. Rasmussen, and M. Blanke, "L1 Adaptive speed control of a small wind energy conversion system for maximum power point tracking," *IEEE Trans. Energy Conver.*, vol. 29, no. 3, pp. 576–584, 2014.
[39] S. Haykin, *Adaptive Filter Theory*. 4th ed. Upper Saddle River, NJ, USA: Prentice-Hall, 2002.
[40] A. H. Sayed, *Adaptive Filters*. Hoboken, NJ, USA: Wiley, 2008.
[41] J. Ni and F. Li, "Efficient implementation of the affine projection sign algorithm," *IEEE Signal Process. Lett.*, vol. 19, no. 1, pp. 24–26, Jan. 2012.
[42] J. M. Gil-Cacho, M. Signoretto, T. van Waterschoot, M. Moonen, and S. H. Jensen, "Nonlinear acoustic echo cancellation based on a sliding-window leaky kernel affine projection algorithm," *IEEE Trans. Audio, Speech, Language Process.(*, vol. 21, no. 9, pp. 1867–1878, Sep. 2013.
[43] K.-A. Lee, W.-S. Gan, and S. M. Kuo, *Subband Adaptive Filtering: Theory and Implementation*. Hoboken, NJ, USA: Wiley, 2009.
[44] H. M. Hasanien, "A set-membership affine projection algorithm-based adaptive-controlled SMES units for wind farms output power smoothing," *IEEE Trans. Sustain. Energy*, vol. 5, no. 4, pp. 1226–1233, Oct. 2014.
[45] H. M. Hasanien, "An adaptive control strategy for low voltage ride through capability enhancement of grid-connected photovoltaic power plants," *IEEE Trans. Power Syst.*, vol. 31, no. 4, pp. 3230–3237, Jul. 2016.
[46] S. M. Muyeen and H. M. Hasanien, "Operation and control of HVDC stations using continuous mixed p-norm-based adaptive fuzzy technique," *IET Gener., Transmiss. Distrib.*, vol. 11, no. 9, pp. 2275–2282, Jun. 2017.
[47] F. Yang, M. Wu, P. Ji, and J. Yang, "An improved multiband-structured subband adaptive filter algorithm," *IEEE Signal Process. Lett.*, vol. 19, no. 10, pp. 647–650, Oct. 2012.
[48] F. Yang, M. Wu, P. Ji, and J. Yang, "Low-complexity implementation of the improved multiband-structured subband adaptive filter algorithm," *IEEE Trans. Signal Process.*, vol. 63, no. 19, pp. 5133–5148, Oct. 2015.
[49] F. Yang, M. Wu, J. Yang, Z. Kuang, and P. Ji, "Transient and steady-state analyses of the improved multiband-structured subband adaptive filter algorithm," *IET Signal Process.*, vol. 9, no. 8, pp. 596–604, Oct. 2015.
[50] H. A. Cabral and M. T. de Melo, "Using genetic algorithms for device modeling," *IEEE Trans. Magn.*, vol. 47, no. 5, pp. 1322–1325, May 2011.
[51] H. Eskandar, A. Sadollah, A. Bahreininejad, and M. Hamdi, "Water cycle algorithm—A novel Metaheuristic optimization method for solving constrained engineering optimization problems," *Comput. Struct.*, vols. 110–111, pp. 151–166, Nov. 2012.
[52] M. A. El-Hameed and A. A. El-Fergany, "Water cycle algorithm-based load frequency controller for interconnected power systems comprising non-linearity," *IET Gener., Transmiss. Distrib.*, vol. 10, no. 15, pp. 3950–3961, Nov. 2016.
[53] A. A. El-Fergany and H. M. Hasanien, "Water cycle algorithm for optimal overcurrent relays coordination in electric power systems," *Soft Comput.*, vol. 23, no. 23, pp. 12761–12778, Dec. 2019.
[54] Y.-S. Kim, I.-Y. Chung, and S.-I. Moon, "Tuning of the PI controller parameters of a PMSG wind turbine to improve control performance under various wind speeds," *Energies*, vol. 8, no. 2, pp. 1406–1425, 2015.
[55] *MATLAB Optimization Toolbox*. London, U.K.: Math Works Press, Aug. 2013.

MAHMOUD A. SOLIMAN was born in Alexandria, Egypt, in December 1986. He received the B.Sc. (Hons.), M.Sc., and Ph.D. degrees in electrical engineering from the Faculty of Engineering, Menoufia University, Shebin El-Kom, Egypt, in 2008, 2013, and 2019, respectively. His Ph.D. research work is focused on the performance enhancement of the wind energy conversion systems.

He joined oil and gas industry as an Electrical Engineer since 2009. Since 2013, he has been engaged in scientific research of power electronics technology and renewable power generation systems. He is currently the Head of the Dynamic Positioning and Navigation Department, Petroleum Marine Services Company, Alexandria, Egypt. His research interests include electrical drives, modern control techniques, power factor correction converters, renewable energy systems, micro- and smart grids, flexible AC transmission systems, HVDC systems, energy storage systems, and artificial intelligence applications on electrical machines and renewable energy systems. He is a Reviewer in different international journals, including the IET and Elsevier journals.

HANY M. HASANIEN (Senior Member, IEEE) received the B.Sc., M.Sc., and Ph.D. degrees in electrical engineering from the Faculty of Engineering, Ain Shams University, Cairo, Egypt, in 1999, 2004, and 2007, respectively. From 2008 to 2011, he was a Joint Researcher with the Kitami Institute of Technology, Kitami, Japan. From 2012 to 2015, he was an Associate Professor with the College of Engineering, King Saud University, Riyadh, Saudi Arabia. He is currently a Professor with the Electrical Power and Machines Department, Faculty of Engineering, Ain Shams University. He has authored, coauthored, and edited three books in the field of electric machines and renewable energy. He has published more than 120 articles in international journals and conferences. His research interests include modern control techniques, power systems dynamics and control, energy storage systems, renewable energy systems, and smart grid. His biography has been included in *Marquis Who's Who in the World* (28 Edition, 2011). He was a recipient of the Encouraging Egypt Award for Engineering Sciences, in 2012. He was awarded the Institutions Egypt Award for Invention and Innovation of Renewable Energy Systems Development, in 2014. He is an Editorial Board Member of *Electric Power Components and Systems Journal*. He is Subject Editor of IET Renewable Power Generation.

AHMED AL-DURRA (Senior Member, IEEE) received the Ph.D. degree in ECE from Ohio State University, in 2010. He is an Associate Professor with the ECE Department, Khalifa University, United Arab Emirates. His research interests are the applications of control and estimation theory on power systems stability, micro and smart grids, renewable energy systems and integration, and process control. He has one U.S. patent, one edited book, 11 book chapters, and over 150 scientific articles in top-tier journals and refereed international conference proceedings. He has successfully accomplished and is currently working on several research projects at international and national levels ($\sim$ 6.5M USD). He has supervised/co-supervised over 20 Ph.D./master's students. He is leading the Energy Systems, Control and Optimization Laboratory, ADNOC Research and Innovation Center. He is an Editor of the IEEE TRANSACTIONS ON SUSTAINABLE ENERGY.

IBRAHIM ALSAIDAN received the B.S. degree from Qassim University, Buraidah, Saudi Arabia, in 2008, and the M.S. and Ph.D. degrees from the University of Denver, in 2012 and 2018, respectively. He joined Qassim University, in 2018, where he is currently an Assistant Professor and the Chair of the Electrical Engineering Department. His current research interests include renewable energy and distributed generation, microgrid, smart grid, power system operation, and planning.